ADVANCED FUNCTIONAL MATERIALS
www.afm-journal.de

www.MaterialsViews.com

Thickness Dependence of the Mechanical Properties of Free-Standing Graphene Oxide Papers

*Tao Gong, Do Van Lam, Renlong Liu, Sejeong Won, Yun Hwangbo, Sanghyuk Kwon, Jinseon Kim, Ke Sun, Jae-Hyun Kim, Seung-Mo Lee, and Changgu Lee**

Graphene oxide (GO) papers are candidates for structural materials in modern technology due to their high specific strength and stiffness. The relationship between their mechanical properties and structure needs to be systematically investigated before they can be applied to the broad range fields where they have potential. Herein, the mechanical properties of GO papers with various thicknesses (0.5–100 μm) are investigated using bulge and tensile test methods; this includes the Young's modulus, fracture strength, fracture strain, and toughness. The Young's modulus, fracture strength, and toughness are found to decrease with increasing thickness, with the first two exhibiting differences by a factor of four. In contrast, the fracture strain slightly increases with thickness. Transmission electron, scanning electron, and atomic force microscopy indicate that the mechanical properties vary with thickness due to variations in the inner structure and surface morphology, such as crack formation and surface roughness. Thicker GO papers are weaker because they contain more voids that are produced during the fabrication process. Surface wrinkles and residual stress are found to result in increased fracture strain. Determination of this structure–property relationship provide improved guidelines for the use of GO-based thin-film materials in mechanical structures.

1. Introduction

Graphene oxide (GO) has been receiving increasing attention from researchers because of its richness of oxygen-containing functional groups on its basal planes and along its sheet edges.[1] These functional groups have a high affinity for water molecules, so GO is hydrophilic and can easily be dispersed in water.[2] The free-standing laminated GO membranes that are prepared from GO solutions can play an important role in many technological applications, including surface coatings,[3] ionic and molecular sieving,[4–6] hydrogen storage,[7,8] transparent and flexible electronics,[9–12] composites,[13,14] micro- and nanoscale devices,[15] and biology and medicine.[16,17] GO papers require certain mechanical properties to provide adequate resistance to the mechanical loads and harsh environments that arise in commercial applications and must retain structural integrity over their lifetimes.

Dikin et al. investigated the mechanical properties of GO papers with thicknesses varying from 2.5 to 25 μm with tensile testing.[2] Kang et al. used nano-indentation on a dynamic contact module system to measure the mechanical properties of 50- and 60-nm-thick GO films.[18] Park et al. characterized the mechanical properties of one, two, and three overlapped layers of GO platelets using atomic force microscopy (AFM).[19] The Young's moduli measured with nanoresonators consisting of thin, stacked GO films were found to surpass values obtained in previous measurements.[20] These results suggest that the mechanical properties of GO films or papers, such as stiffness and fracture strength, might vary with thickness; however, no systematic study of this issue has been carried out to date.

T. Gong, K. Sun, Prof. C. Lee
SKKU Advanced Institute of Nano Technology (SAINT)
Sungkyunkwan University
2066, Seobu-ro, Jangan-gu, Suwon, Gyeonggi 440–746, South Korea
E-mail: peterlee@skku.edu
D. V. Lam, Prof. S.-M. Lee
Nanomechatronics, Korea University of Science and Technology (UST)
217 Gajeong-ro, Yuseong-gu, Daejeon 305–333, South Korea
D. V. Lam, Dr. Y. Hwangbo, Prof. J.-H. Kim, Prof. S.-M. Lee
Department of Nanomechanics
Nano-Mechanical Systems Research Division
Korea Institute of Machinery & Materials (KIMM)
156 Gajungbukno, Yuseong-gu, Daejeon 305–343, South Korea
R. Liu, S. Kwon, Dr. J. Kim, Prof. C. Lee
School of Mechanical Engineering
Sungkyunkwan University
2066, Seobu-ro, Jangan-gu, Suwon, Gyeonggi 440–746, South Korea
Dr. S. Won
Department of Mechanical Engineering
Korea Advanced Institute of
Science & Technology (KAIST)
291 Daehak-ro, Yuseong-gu, Daejeon 305–701, South Korea

DOI: 10.1002/adfm.201500998

Since GO papers have significant potential for a variety of applications as mentioned above—especially as structural materials, the dependence of their mechanical properties on thickness should be characterized. Additionally, because a property such as Young's modulus is well known to be independent of the material's size, discovering the mechanism behind this phenomenon will give us insight into the material behavior at the low-dimensional limit for this new type of layered structure with nanosized elements, whose properties on scale-dependence have rarely been previously explored. In this study, we measured the Young's modulus, fracture strength, fracture strain, and fracture toughness of free-standing GO papers with thicknesses in the range 0.5 to 100 μm using tensile and bulge test methods. Interestingly, these properties were found to all depend on thickness. Using transmission electron microscopy (TEM), scanning electron microscopy (SEM), and AFM, we determined how the mechanical properties of the GO papers vary with thickness. An understanding of the mechanism behind the structural assembly of GO papers and that of their macro- and microstructures, could lead to efficient membrane fabrication and improved mechanical properties, enabling the practical application of GO in various fields.

2. Results and Discussion

GO papers with various thicknesses were fabricated by filtering GO solutions of various concentrations through aluminum oxide filter membranes (Anodisc, Whatman, cat. no. 6809–5012). Each GO paper was peeled off from the membrane and cut into rectangular strips with a width of 2 mm and lengths in the range of 20 to 30 mm (**Figure 1**a–c and Figure S1 in the Supporting Information (SI)) using laser cutting for the tensile test, which is described below. Because of the functional groups in GO, its mechanical properties will vary as a result of the humidity in air. In order to avoid the inconsistency of data due to atmospheric humidity, we kept our samples in a vacuum chamber for weeks to prevent excessive exposure to moisture. Also we prepared the samples and performed the experiments in an environment where the temperature and humidity were maintained constant.

Figure 1d and e show schematic diagrams of the bulge and tensile test set-ups, respectively. Thick GO papers (thicker than 2 μm) were characterized with the tensile test method. The tensile tests were carried out using a microtester (Deben, N200) (Figure S2a, SI) with a constant displacement rate of 1.7 μm s^{-1}. The gap between the clamps was 12 mm. The fracture strength and strain were recorded as the highest values obtained when fracture occurs, and the Young's modulus and fracture toughness were calculated from the slope of the stress–strain curve and from the product of the measured fracture stress and strain, respectively (Figure S3, SI).

In general, the strip-type specimen has been widely adapted for the tensile test of GO papers.[2,21–23] If the design of the specimen—e.g., length-to-width ratio—is not suitable, the fracture strength cannot be measured precisely because strain distribution will not be uniform over the gauge length as a result of the large effect of grip confinement. It has also been reported that strain distribution within the gauge length of a specimen becomes uniform when the length-to-width ratio of a specimen is higher than 4.[24] In our experiments, we fixed the gauge length for specimens to 12 mm to adapt it to the experimental set-up and chose the width to be 2 mm for minimum deviation of strain within the gauge length in order to obtain more accurate mechanical properties. We evaluated the compatibility of the specimen using a finite element analysis tool (Abaqus) and found that strain is uniform in the gauge length region with a negligible difference between the strain in gauge length and the grip-to-grip strain. In this experiment, proper gripping force was also required to avoid sample sliding at the grip or specimen

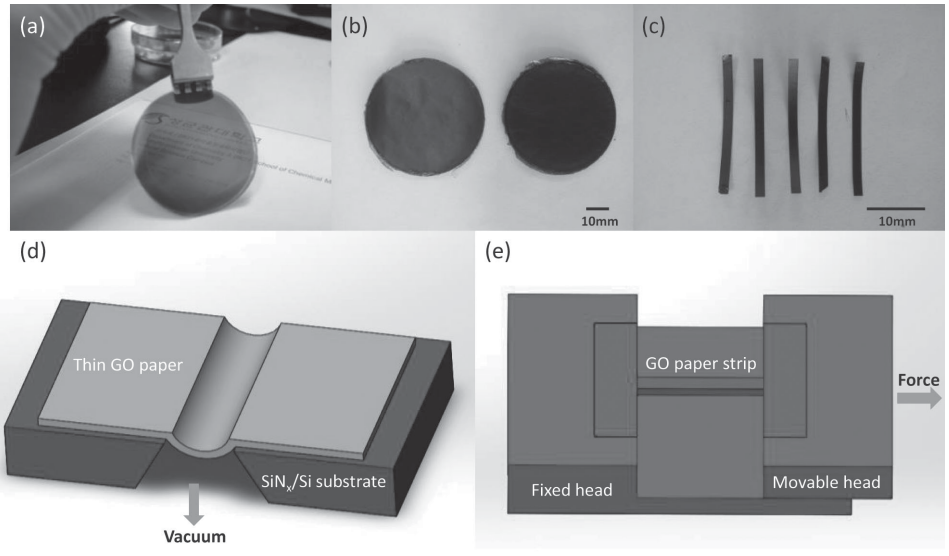

Figure 1. GO samples and mechanical testing methods. a) Transparent thin GO papers for the bulge test. b) Free-standing thick GO papers with a diameter of 47 mm. c) Laser-cut GO strips. d) Schematic diagram of the set-up for the bulge test for thin (<2 μm) GO samples. e) Schematic diagram of the tensile testing apparatus for the thick (≥2 μm) GO paper strips.

fractures near the grip. When the sample thickness increases, the gripping force also increases to counter the sample sliding, but it should not be strong enough to cause sample damage near the grip. For a specific thickness, we repeated the tensile tests on at least 5 samples, and we observed that most of the specimens fractured within the gauge length area and that no sliding occurred. In addition, we could see that the deviation in mechanical properties is not so significant for each thickness.

The tensile test method is suitable for thick samples, but it is not applicable to films thinner than 2 μm, which are too brittle to be clamped to the measurement apparatus. Furthermore, since thinner GO papers (less than 2 μm) are fragile, it is difficult to prepare thin strips for tensile testing; hence, it was necessary to use the bulge test for thinner samples.

For the bulge test, since the length-to-width ratio of the slit in the SiN_x/Si substrate D/b(12/2) (Figure S2b–d, SI) is greater than 4, it can be assumed that the membrane is under plane strain.[25] In this case, the stress (σ) and strain (ε) of the membrane can be expressed as

$$\sigma = \frac{pD^2}{8tH} \tag{1}$$

$$\varepsilon = \frac{8H^2}{3D^2} \tag{2}$$

where p, D, H, and t are the pressure, slit width, height of the bulged membrane, and membrane thickness, respectively. The stress–strain relationship is given by the following equation:

$$\sigma = \frac{E}{1-\nu^2}\cdot(\varepsilon+\varepsilon_0) = \frac{E}{1-\nu^2}\cdot\varepsilon+\sigma_0 \tag{3}$$

where E, ε_0, and σ_0 are the Young's modulus, residual strain, and residual stress, respectively. Assuming that Poisson's ratio $\nu = 0.165$ and fitting Equation (3) to the stress–strain data from Equation (1) and (2),[26] the Young's modulus and the residual stress can be determined.

By using these two methods, we obtained the Young's modulus, fracture strength, fracture strain, and fracture toughness of GO papers for various thicknesses, as shown in **Figure 2**. The Young's modulus and the fracture strength decrease with increasing thickness. The Young's modulus and the fracture strength of the thinnest sample (0.5 μm) are approximately four times the values of the thickest sample (100 μm). On the other hand, the fracture strain appears to increase with thickness; however, in contrast to the trends of the other properties, this increase is quite small, and the dependence on the thickness is weaker. The fracture toughness appears to slightly decrease with increasing thickness. Since the fracture strain does not vary much with thickness, the fracture toughness is expected to decrease with thickness. According to conventional fracture mechanics theory, a material's fracture strength is expected to decrease with increasing thickness due to the resulting increase in the number of defect sites, which increases the possibility of crack initiation.[27] The trend in the fracture strength results appears to follow the predictions of this theory; however, the Young's modulus does not usually depend on thickness since it is a material's intrinsic property, which is not significantly

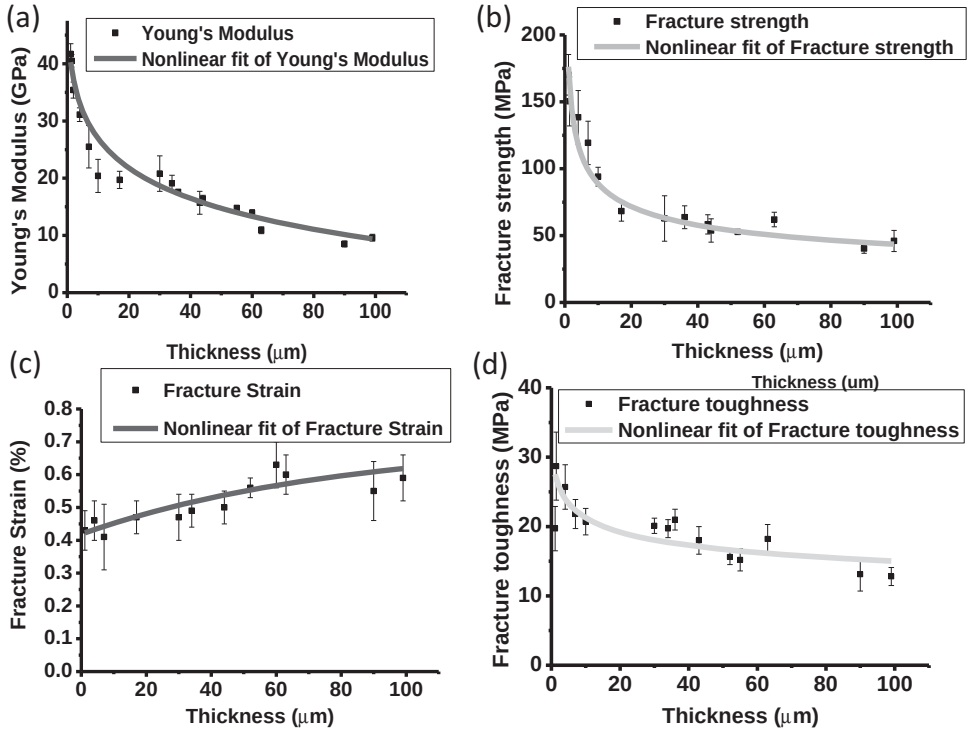

Figure 2. The mechanical properties of the GO papers with various thicknesses. The standard deviation (±s.d.) is displayed at each data point. a) Young's modulus, b) fracture strength, c) fracture strain, and d) fracture toughness.

affected by defects. There have been some reports of the thickness dependence of the Young's modulus of some materials;[28–31] however, these materials were all of nanometer-scale thickness less than 100 nm, unlike the materials examined in our study. At the nanoscale, unbound atoms and surface contamination have significant influence on mechanical properties. At the micro- and macroscale however, such surface effects are usually negligible due to the decreased surface-to-volume ratio. As a result, this type of thickness dependence is unexpected for the materials considered in our study. Since GO paper is not crystalline or a highly ordered material—but rather a metamaterial consisting of a random stack of microsized flakes, we speculate that its stack structure might affect its mechanical properties.

In order to investigate the thickness dependence of the mechanical properties of the GO papers, we characterized their micro- and nanostructures. We first determined the spacings between the stacked layers of GO in the papers with X-ray diffraction (XRD); the stack spacing can reflect the strength of the bond between the layers and affect the stiffness and strength of a layered structure. There was little variation however in the measured spacing data with thickness (Figure S4, SI), so the spacing does not seem to be related to the mechanical properties. Since the GO papers attached to the Anodisc membrane were sucked by the aspirator and have different expansion coefficients, these free-standing thin films are subjected to significant stress during drying and the separation from the Anodisc membranes, which could cause fracture, deformation, or some other type of defect in their structures. Visible wrinkles or deformations can manifest in the GO papers, especially the thicker ones, due to the preparation process.

TEM was used to examine the microstructures of the GO papers. The lamella structure of each GO sample was cut into small pieces and the cross-section of the GO paper was thinned with a focused ion beam (FIB) and then extracted and welded onto a Cu TEM grid with 4 posts using an omniprobe. Finally, we examined the cross-sections of the lamella GO samples with TEM. In **Figure 3**, the TEM images show that there are vacancies in the lamella structures of all the GO samples; however, in the thinnest sample, the length and thickness of the vacancies are much smaller than those of the thicker samples. Furthermore, the density of the defects is lower for the thinner samples. This kind of defect in the lamella structures is likely to have been generated during the preparation of the GO papers (**Figure 4**). During this process, the vacuum pump generates a pressure difference across the filter membrane, and water passes through the filter membrane while the GO flakes stack over time. During filtration, the membrane is expected to bend due to the pressure difference. After filtration, the pressure difference is removed; hence, the (GO paper)/Anodisc stack tries to return to a flat shape. Since the GO paper was synthesized with a bent structure, a bending stress is generated in the paper, and ripples are formed. Since the bonding energy between the GO flake layers is relatively low, delamination or cracking can occur, which leads to the formation of vacancies. Since the stored shear strain energy is higher in the thick papers, the voids from the delamination should be larger than those of thinner papers, as can be seen in Figure 3.

We also used SEM and AFM imaging in our surface structure investigation. The SEM and AFM images reveal that the roughness of the GO papers increases with their thickness (**Figure 5**). At the first stage, as shown in Figure 4, the water will penetrate the membrane fast because there is no GO paper formed. Once the GO flakes stack, the flow path is blocked, and the vertical flow rate will decrease with increasing thickness of the GO. When the fluid flow is blocked by the GO paper, it is expected to try to find a flow path with less resistance, and the lateral direction flow velocity, which we denote 'lateral disturbance', increases. This lateral disturbance will cause wrinkle formation and an increase in the roughness of the surface with increasing thickness of the GO paper due to the reduced stacking speed as shown in **Figure 6**. It is common sense that the fabrication of thicker GO papers requires more time than that of thinner ones, which means that the residual stress of thicker GO papers is larger than that of thinner ones. It is well known that the bulk strain has a significant influence on the structure of the surface. A rough surface has a larger surface area and a higher surface free energy as a consequence of bulk strain, which is counteracted by a reduction in the strain energy near the surface.[32,33]

According to the conventional theories of buckling of thin films on top of bulk materials, its wavelength is proportional to the thickness.[34,35] Our result is the opposite because the wavelength increases with decreasing thickness as shown in **Figure 7**. Hence, the thickness dependence of the wavelength should be explained with another mechanism. As explained above, the voids are formed during the fabrication of GO papers, and they are larger in thicker samples. As a result, the increased void size in thicker papers makes them more corrugated. The corrugation structure inside the papers should influence the fracture strain because the papers with more corrugation will be stretched further, like springs before fracture. Figure 7 also shows that the corrugation in the paper increases the roughness on the surface by raising a long-range undulation level; hence, it appears that the surface wrinkles,

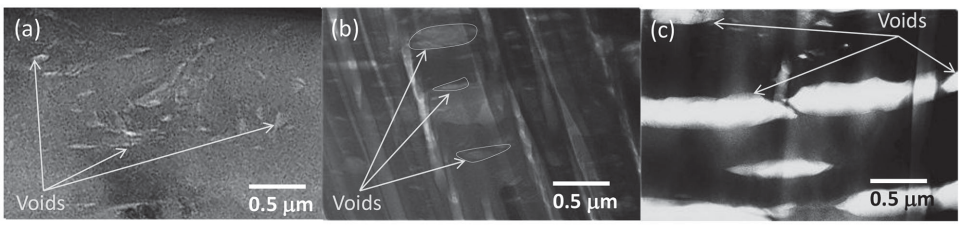

Figure 3. Cross-sectional TEM images of GO papers with various thicknesses: a) 2, b) 52, and c) 100 μm. The slashes in (b) are due to the FIB thinning process. The circles are visual guides indicating the voids.

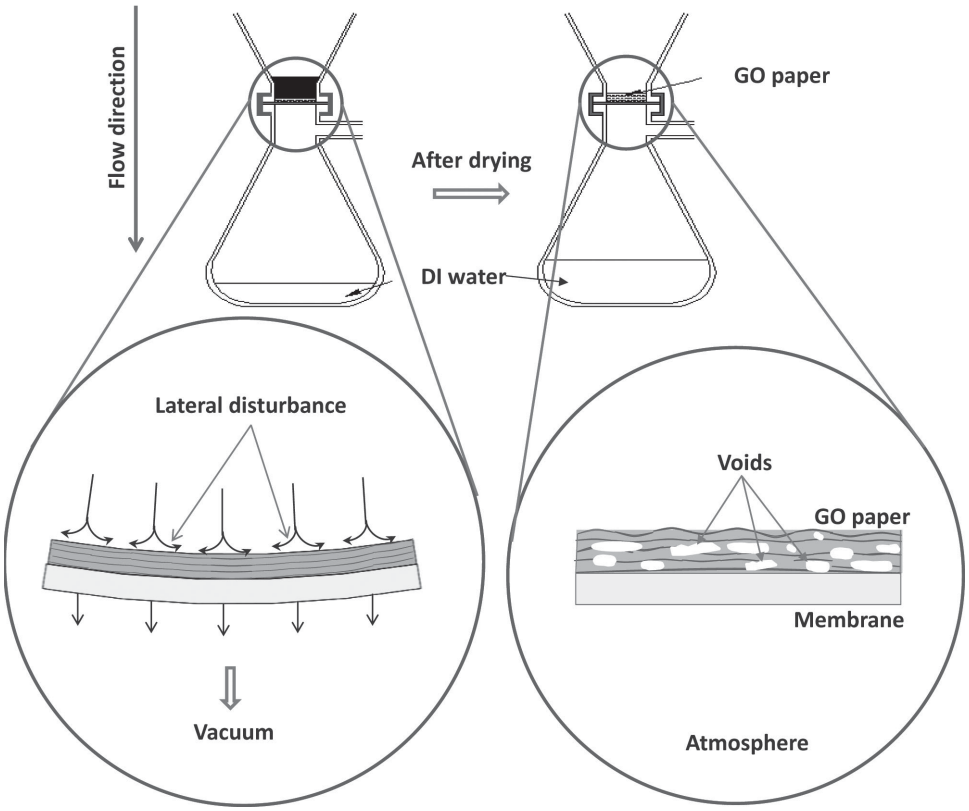

Figure 4. Presumable formation of the structural defects in GO paper during fabrication using the vacuum-assisted filtration.

the voids in the bulk, and the corrugation structure affect each other's formation along with the mechanical properties of GO paper.

Of the three structural factors that are likely to affect the mechanical properties of GO papers, we propose that the voids inside the GO papers are the dominant influence. The surface wrinkles act as surface defects that mainly reduce the fracture strength, but not significantly, and the corrugation structure lowers the Young's modulus, but not the fracture strength. In contrast, the voids in a paper decrease both its Young's modulus

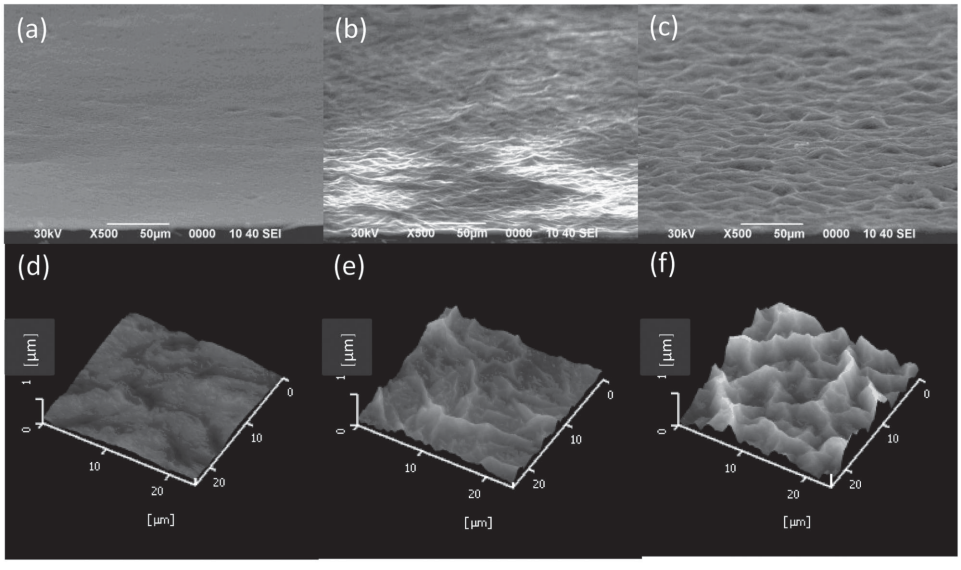

Figure 5. a–c) SEM images of the surfaces of GO samples with a thickness of a) 4, b) 36, and c) 63 μm, and d–f) AFM roughness images of d) 4, e) 36, and f) 63 μm. The arithmetic averages of the absolute values of the surface roughness of the GO papers are 47.8, 68.89, and 153.8 nm, respectively.

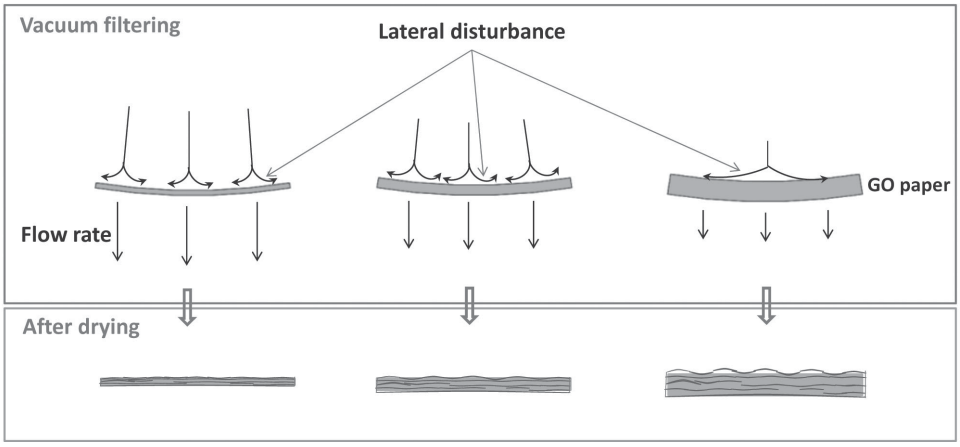

Figure 6. Suggested mechanism of the thickness-dependent wrinkle formation on the surface of GO papers.

and its fracture strength at the same time because they weaken the overall structure.

We can treat the voids as pores in a porous structure and apply models that relate such porosity to the mechanical properties of materials. The Young's modulus (E) and the fracture strength (S) of porous materials can be described by using the Spriggs[36] and Ryshkewitch–Duckworth[37] equations

$$E = E_0 \cdot e^{(-b \cdot p)} \tag{4}$$

$$S = S_0 \cdot e^{(-a \cdot p)} \tag{5}$$

respectively, where E_0 is the zero-porosity Young's modulus and S_0 is the zero-porosity fracture strength, a and b are material constants, and P is the volume-fraction porosity. The material constants describe the bonding capacity of the material and indicate the effects of a change in porosity on the fracture strength and the Young's modulus. By fitting the measured data, we obtained values of 6.35 and 5.64 for a and b, respectively, and 46.68 GPa and 181.56 MPa for E_0 and S_0, respectively. Here, E_0 and S_0 are the maximum Young's modulus and fracture strength, respectively, of the material without any voids. In GO papers, these values can be achieved when the thickness approaches zero, which means there are no cracks or voids due to delamination in the lamellar structure.

We obtained the volume-fraction porosities of the papers by measuring their masses and volumes and comparing their densities with GO particles, which do not contain voids. **Figure 8** shows that the porosity increases with thickness and saturates above 60 μm. The trend in the saturation exactly follows those for the Young's modulus and the fracture strength. At a thickness of 100 μm, the porosity is approximately 27%, which indicates that thick GO papers contain significant voids in their lamellar structures. This dependence of the porosity on thickness supports our argument that the voids in the GO papers are the main contributor to the variation in their mechanical properties.

3. Conclusion

We have characterized the thickness dependence of the mechanical properties GO papers; these include the Young's modulus, fracture strength, fracture strain, and fracture toughness. The Young's modulus and fracture strength were found to decrease with thickness, ranging from ≈44.6 to ≈8.5 GPa and from ≈170.2 to ≈40 MPa, respectively. The macrostructure, microstructure, and surface morphology—such as crack formation, roughness change, and corrugation—are the factors that determine the variations of the mechanical properties of GO papers with differing thicknesses. The porosity data revealed that the voids in the GO papers are closely associated with the trends in the mechanical properties, and thus are the main contributing factor to these variations. Surface roughness and corrugation structure however also weaken the GO papers or make them less stiff. In particular, corrugations in the bulk increase the fracture strain because the paper becomes more stretched

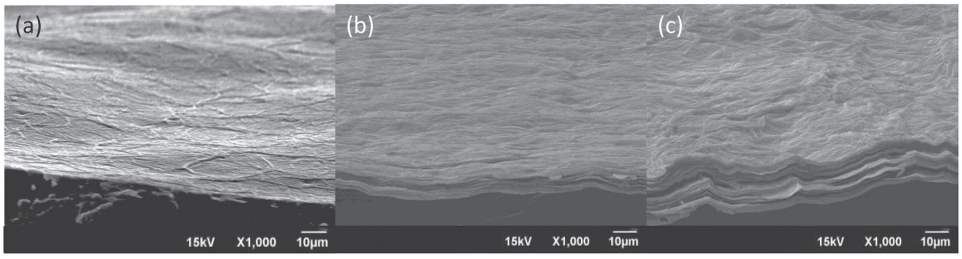

Figure 7. Cross-sectional SEM images of GO samples showing corrugation structures with varying thicknesses: a) 2, b) 8, and c) 22 μm.

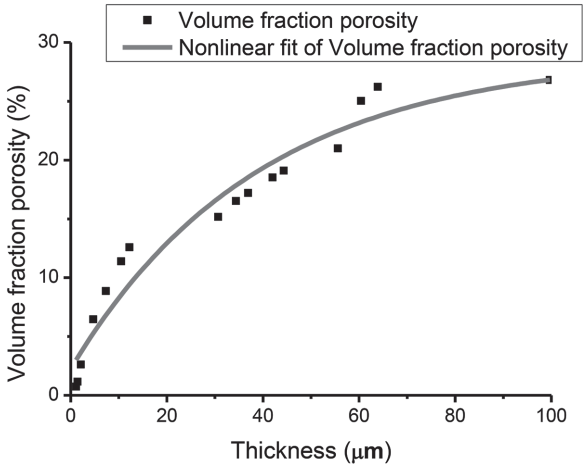

Figure 8. Thickness dependence of the volume-fraction porosities of the GO papers.

under load. This study has provided significant insights into the relationship between the manufacturing process, structure, and mechanical properties of stacked materials. As a result, we envision that by modifying the fabrication process, such as by varying the filtration speed, filter material, and GO properties, the mechanical properties of GO papers can be controlled for a diverse range of applications.

4. Experimental Section

Preparation of the GO Solution: The GO solution was prepared from natural graphite flakes using the modified Hummer method (Figure S1a, SI). Graphite (12 g; Alfa Aesar, 99.8%, 325 mesh), 740 mL of H_2SO_4 (purity 95%), and 10 g of $NaNO_3$ were successively added to a beaker with a magnetic stirrer. $KMnO_4$ (48 g) was slowly added into this mixture after 1 h of cooling in an ice-water bath. The mixture was stirred until it became a highly viscous liquid at room temperature. A H_2SO_4 aqueous solution (1200 mL; 5 wt%) was added to the above solution, which was then stirred for 1 h. Then, 30 wt% H_2O_2 aqueous solution was slowly added until the mixture became yellow, which was then stirred for another 1 h. The products were washed more than 15 times using a mixture of 5 wt% H_2O_2 and 3 wt% H_2SO_4, and then they were washed with deionized (DI) water until neutral to obtain the GO solution. The concentration of the resulting GO aqueous solution was approximately 20 mg mL^{-1} (Figure S1a inset, SI). This solution was sonicated for 5–10 min until the GO was dispersed in the DI water into individual sheets (Figure S5, SI) with an average lateral dimension of more than 1 μm and that remained stable in vials for longer than one year (see the inset in Figure S1a inset, SI).

Preparation of GO Papers: GO papers with various thicknesses were fabricated by performing vacuum-assisted filtration of the GO solutions with various concentrations through an Anodisc membrane (Whatman, diameter 47 mm, pore size 0.2 μm). The duration of the whole filtration process was 6 h to one week, depending on the desired thickness, which ranged from hundreds of nanometers to hundreds of micrometers. In the initial state, the GO flakes assemble on the membrane very rapidly due to the vertical water flow. Once a thin GO film has formed, the water flow becomes slower and slower due to the clogging of the filter by the deposition of GO sheets. The structure of the top layer of GO paper is not as ordered and dense as that of the bottom layer because the water flow becomes slower and evaporation occurs at the end point from the top.[2] Furthermore, the increase in thickness with deposition of the GO thin film means that the pressure varies throughout the whole process. The residual stress persists in the GO papers, especially in the thicker ones.

Preparation of GO Strips: Samples with various thicknesses for tensile testing were cut into rectangular strips (Figure S1c, SI) with a width of 2 mm and lengths in the range of 20–30 mm by using laser cutting, which results in less mechanical damage or microdefects than cutting with scissor or a razor blade; this enables precise control of the sample width (Figure S1c inset, SI). A micrometer (Mitutoyo) with a minimum resolution of 1 μm was used to measure the samples with thicknesses above 10 μm. The thicknesses of thinner samples were measured with field-effect SEM (FESEM; JEOL, JSM-700F).

Tensile Test Device: As mentioned in the Results and Discussion section, the mechanical properties of thicker strips were measured by performing tensile tests. Uniaxial tensile measurements were carried out under room conditions with a gap between the clamps of 12 mm (Figure S2a, SI). The fracture strength was recorded as the highest stress obtained, and the stiffness was calculated from the slope of the stress–strain curve (Figure S3, SI) after initial strain hardening for all samples.

Bulge Test Device: The thinner GO papers were cut into specimens with areas of 16 mm × 16 mm. The samples were attached to a Si substrate with a hole size of 2 mm × 12 mm using epoxy (Figure S2b, SI).

Computational Details: The mass (m) of each GO paper was measured with an electronic balance (Table S1, SI). The volume (v) of each GO paper was measured by using Archimedes' method in oil. The densities of the papers with various thicknesses were calculated using the equation $\rho_{bulk} = m/v$. Additionally, the density of the GO particles could be calculated by drying the GO solution at room temperature under vacuum until no further weight loss was observed. A value for the porosity (Table S1, SI) can be calculated from the bulk density ρ_{bulk} and the particle density $\rho_{particle}$:

$$P = 1 - \frac{\rho_{bulk}}{\rho_{particle}} \quad (6)$$

XRD: Thin-film XRD (SmartLab, Rigaku) was used to determine the crystallinity and structural variations in the GO membranes. The layered structures of the GO papers were revealed in the XRD spectra (Figure S4, SI). The peak in the spectrum of a GO paper specimen corresponds to the average layer distance. There are no significant differences between the spectra of the samples. The average d-spacing is 0.78 nm.

AFM: AFM was carried out using an SII NanoTechnology Inc. SPI 4000 in tapping mode. The resulting images shows that the majority of the GO flakes synthesized with the modified Hummers method are significantly larger than 1 μm and that the thickness of the monolayer is approximately 1 nm (Figure S5, SI).

X-Ray Photoelectron Spectroscopy (XPS): XPS was performed using a monochromatic Al Kα X-ray source (K-Alpha, Thermoscientific). The spot size of each measurement was 0.5 μm^2. In the high-resolution XPS spectra (Figure S6, SI), the C 1s spectrum for GO clearly shows that it contains four kinds of carbon atoms in different functional groups, namely C–C (284.6 eV), C–O (286.8 eV), carbonyl C = O (288.5 eV), and carboxylate O = C–O (290.2 eV).[14]

Raman Spectroscopy: A Raman spectrometer (LabRam ARAMIS) equipped with a 514-nm laser line and a 100× objective was used in this study. The back-scattered Raman light was diffracted by 1800 gratings per millimeter. To avoid local heating effects, the laser power density was kept below 100 μW μm^{-2}. The typical GO Raman spectrometer can be seen in the SI (Figure S7).

Supporting Information

Supporting Information is available from the Wiley Online Library or from the author.

Acknowledgements

T.G. and D.V.L. contributed equally to this work. This study was supported by the Basic Science Research Program (2011–0014209,

2009–0083540) and the Global Frontier Research Center for Advanced Soft Electronics (2011–0031630) through a National Research Foundation of Korea Grant funded by the Korean government Ministry of Science, ICT and Future Planning.

Received: March 13, 2015
Revised: April 15, 2015
Published online: May 12, 2015

[1] K. P. Loh, Q. Bao, G. Eda, M. Chhowalla, *Nat. Chem.* **2010**, *2*, 1015.
[2] D. A. Dikin, S. Stankovich, E. J. Zimney, R. D. Piner, G. H. B. Dommett, G. Evmenenko, S. T. Nguyen, R. S. Ruoff, *Nature* **2007**, *448*, 457.
[3] K. Yang, J. Wan, S. Zhang, B. Tian, Y. Zhang, Z. Liu, *Biomaterials* **2012**, *33*, 2206.
[4] H. Li, Z. Song, X. Zhang, Y. Huang, S. Li, Y. Mao, H. J. Ploehn, Y. Bao, M. Yu, *Science* **2013**, *342*, 95.
[5] R. K. Joshi, P. Carbone, F. C. Wang, V. G. Kravets, Y. Su, I. V. Grigorieva, H. A. Wu, A. K. Geim, R. R. Nair, *Science* **2014**, *343*, 752.
[6] D. V. Lam, T. Gong, S. Won, J. H. Kim, H. Lee, C. Lee, S. M. Lee, *Chem. Commun.* **2015**, *51*, 2671.
[7] R. T. Yang, *Carbon* **2000**, *38*, 623.
[8] L. Schlapbach, A. Züttel, *Nature* **2001**, *414*, 353.
[9] G. Eda, G. Fanchini, M. Chhowalla, *Nat. Nanotechnol.* **2008**, *3*, 270.
[10] K. S. Kim, Y. Zhao, H. Jang, S. Y. Lee, J. M. Kim, K. S. Kim, J. H. Ahn, P. Kim, J. Y. Choi, B. H. Hong, *Nature* **2009**, *457*, 706.
[11] Z. Wei, D. Wang, S. Kim, S. Y. Kim, Y. Hu, M. K. Yakes, A. R. Laracuente, Z. Dai, S. R. Marder, C. Berger, *Science* **2010**, *328*, 1373.
[12] S. Pei, J. Zhao, J. Du, W. Ren, H. M. Cheng, *Carbon* **2010**, *48*, 4466.
[13] S. Stankovich, D. A. Dikin, G. H. B. Dommett, K. M. Kohlhaas, E. J. Zimney, E. A. Stach, R. D. Piner, S. T. Nguyen, R. S. Ruoff, *Nature* **2006**, *442*, 282.
[14] H. Qin, T. Gong, Y. Cho, C. Lee, T. Kim, *Polym. Chem.* **2014**, *5*, 4466.
[15] O. C. Compton, D. A. Dikin, K. W. Putz, L. C. Brinson, S. T. Nguyen, *Adv. Mater.* **2010**, *22*, 892.
[16] Y. Wang, Z. Li, D. Hu, C. T. Lin, J. Li, Y. Lin, *J. Am. Chem. Soc.* **2010**, *132*, 9274.
[17] X. Sun, Z. Liu, K. Welsher, J. T. Robinson, A. Goodwin, S. Zaric, H. Dai, *Nano Res.* **2008**, *1*, 203.
[18] S. H. Kang, T. H. Fang, Z. H. Hong, C. H. Chuang, *Diamond Related Mater.* **2013**, *38*, 73.
[19] S. Park, K. S. Lee, G. Bozoklu, W. Cai, S. T. Nguyen, R. S. Ruoff, *ACS Nano* **2008**, *2*, 572.
[20] J. T. Robinson, M. Zalalutdinov, J. W. Baldwin, E. S. Snow, Z. Wei, P. Sheehan, B. H. Houston, *Nano Lett.* **2008**, *8*, 3441.
[21] D. S. Dugdale, *J. Mech. Phys. Solids* **1960**, *8*, 100.
[22] T. Haga, *J. Mater. Process. Technol.* **2002**, *130*, 558.
[23] Y. Saito, H. Utsunomiya, N. Tsuji, T. Sakai, *Acta Mater.* **1999**, *47*, 579.
[24] J. R. Davis, *Tensile Testing*, 2nd ed., ASM International, Materials Park, OH **2004**, p 112.
[25] Y. Xiang, X. Chen, J. J. Vlassak, *J. Mater. Res.* **2005**, *20*, 2360.
[26] O. L. Blakslee, D. G. Proctor, E. J. Seldin, G. B. Spence, T. Weng, *J. Appl. Phys.* **1970**, *41*, 3373.
[27] A. A. Griffith, *Philos. Trans. R. Soc. London A* **1921**, *221*, 163.
[28] J. M. Torres, N. Bakken, C. M. Stafford, J. Li, B. D. Vogt, *Soft Matter* **2010**, *6*, 5783.
[29] A. I. Fedorchenko, A. B. Wang, H. H. Cheng, *Appl. Phys. Lett.* **2009**, *94*, 152111.
[30] A. Mathur, J. Erlebacher, *Appl. Phys. Lett.* **2007**, *90*, 061910.
[31] K. B. Gavan, H. J. R. Westra, E. W. J. M. van der Drift, W. J. Venstra, H. S. J. van der Zant, *Appl. Phys. Lett.* **2009**, *94*, 233108.
[32] R. M. Spriggs, *J. Am. Ceram. Soc.* **1961**, *44*, 628.
[33] W. Duckworth, *J. Am. Ceram. Soc.* **1953**, *36*, 68.
[34] D. Schneider, T. Schwarz, B. Schultrich, *Thin Soild Films* **1992**, *219*, 92.
[35] A. J. Nolte, M. F. Rubner, R. E. Cohen, *Macromolecules* **2005**, *38*, 5367.
[36] Y. W. Mo, D. E. Savage, B. S. Swartzentruber, M. G. Lagally, *Phys. Rev. Lett.* **1990**, *65*, 1020.
[37] Y. H. Xie, G. H. Gilmer, C. Roland, P. J. Silverman, S. K. Buratto, J. Y. Cheng, E. A. Fitzgerald, A. R. Kortan, S. Schuppler, M. A. Marcus, *Phys. Rev. Lett.* **1994**, *73*, 3006.